Full wave analysis of arbitrarily shaped line-fed microstrip antennas using triangular finite-element method

K.-L. Wu, PhD
J. Litva, PhD
R. Fralich, MEng
C. Wu, MSc

Indexing terms: Antennas (microstrip), Numerical analysis

Abstract: A numerical method is developed to investigate arbitrarily-shaped line-fed microstrip antennas. The electric integral equation is solved by adopting the triangular shaped basis element and using the Galerkin procedure. In the integral equation, Sommerfeld-type full wave Green's functions are used. To enhance the computational efficiency, the full wave discrete image technique is applied. To examine the method, comparison is made between numerical and experimental results which show excellent agreement. The experimental error is also discussed.

1 Introduction

Microstrip antennas have been the subject of a great deal of theoretical and experimental attention in the past decade because they possess a number of desirable attributes. Owing to these attributes, the antennas can be used to good advantage in a number of applications, in particular aerospace systems where weight is usually a critical factor. Most of the recent development in the accurate analysis of microstrip antennas is based on full-wave techniques, where the spectral domain dyadic Green's function is used to describe the antenna's electromagnetic fields. The derived fields consist of both surface-wave and radiated fields. Most of these techniques, though, are restricted to the analysis of rectangular shaped patch antennas, i.e. patches with right-angle step boundaries [1, 2]. This restriction is due to their formulation being based on rectangular-shaped subdomain or entire-domain basis functions. The application of microstrip antennas to sophisticated antenna systems requires innovation in the use of novel patch geometries. For example, a compact dual-frequency antenna, may require the use of a circular-ring microstrip antenna combined with one or more patch radiating elements. Furthermore, some patch geometries, such as triangles and circles, may be used for some practical reasons such as polarisation, scanning, space or bandwidth considerations. The efficient incorporation of these complex geometries into antenna designs; in particular, array antennas, requires the development of a rigorous numerical model. It follows then that an accurate numerical model which can efficiently handle arbitrarily shaped microstrip antennas is increasingly becoming a requirement for designing sophisticated antenna systems.

A number of sophisticated numerical techniques have been developed and used to analyse irregularly shaped microstrip antennas or resonators [3]. At best, most of these techniques, such as the cavity and modal expansion models [4, 5, 6], the Neuman boundary based finite element model [3] and the generalised edge boundary condition model [7], provide only approximate solutions. The techniques are usually based on impractical assumptions and are difficult to use in multilayered problems. Despite the approximate nature of their solutions, for certain configurations they yield results that agree fairly well with experimental measurements. They have an inherent limitation, though, as they can only be applied to simple shapes or thin substrates. It is difficult, for example, to analyse coupling between patch antennas and complex feeding structures, such as those used in the case of proximity coupled patch antennas. A rigorous technique was proposed for analysing circular patch antennas [8]. The model uses an exact Fourier-transformed dyadic Green's function, thereby ensuring that all of the information that is inherent to full-wave techniques is brought to bear on the problem. Recently, this technique has been extended to more complicated structures, such as rectangles, circular discs and equilateral triangles [9]. However, patch shapes which are amenable to analysis using this technique are limited to those whose eigenfunctions are known.

The analysis to be presented here will focus on patch antennas with arbitrary shapes and which are fed by microstrip transmission lines. The reasons for this choice of topic are:

(*a*) this feed arrangement is widely used in practical array designs

(*b*) no impractical assumptions need be made, such as the requirement that the substrate be thin

(*c*) any added complexity that might result with the addition of a probe feed-model is avoided.

The model can be applied to all microstrip antennas that use microstrip line feeds, such as edge-feeds, capacitive gap-feeds and electromagnetic coupling-feeds.

The integral equation for the unknown current on both the patch and the microstrip feedline is formulated

Paper 8099H (E11), received 11th March 1991

The authors are with the Communications Research Laboratory, McMaster University, Ontario, Canada, L85 4KI

in Section 2. Next, the vector-current basis functions are introduced and used to discretise the integral equations. The conventional Galerkin's procedure is then called upon to derive the final matrix equation; this is then used to solve for the currents on both the patch and its attending feed lines.

The potential Green's functions for an electric horizontal dipole embedded in a microstrip dielectric are defined in Section 3, in terms of Sommerfeld-type integrals. To enable these integrals to be calculated in an efficient manner, the full-wave discrete image technique [10] is adopted and its range of applicability is extended to treat the case of very thin substrates.

2 Basic formulas for analysis

Let S denote the surface of the patch antenna and its feeding networks, as shown in Fig. 1 and $\boldsymbol{n}$ denote the

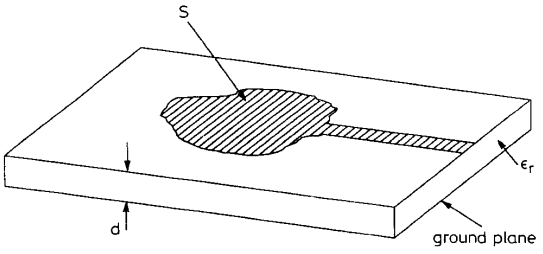

Fig. 1 *An arbitrarily shaped microstrip antenna*

unit normal. The electric field integral equation is used in this analysis by applying the boundary condition $\boldsymbol{n} \times (\boldsymbol{E}^i + \boldsymbol{E}^s) = 0$ on S, i.e.

$$-\boldsymbol{n} \times \boldsymbol{E}^i = \boldsymbol{n} \times (-j\omega \boldsymbol{A} - \nabla\Phi), \quad \boldsymbol{r} \text{ on } S \tag{1}$$

with the magnetic vector potential defined by

$$\boldsymbol{A}(\boldsymbol{r}) = \frac{\mu}{4\pi} \iint_S \boldsymbol{J}(\boldsymbol{r}') \cdot \overleftrightarrow{G}_A(\boldsymbol{r}, \boldsymbol{r}')\, dS' \tag{2}$$

and the charge scalar potential by

$$\Phi(\boldsymbol{r}) = \frac{1}{4\pi\varepsilon} \iint_S \sigma(\boldsymbol{r}') G_q(\boldsymbol{r}, \boldsymbol{r}')\, dS' \tag{3}$$

where $\overleftrightarrow{G}_A(\boldsymbol{r}, \boldsymbol{r}')$ is the dyadic Green's function for the magnetic vector potential and $G_q(\boldsymbol{r}, \boldsymbol{r}')$ is the scalar Green's function for the charge scalar potential. Both of the Green's functions will be defined to take into account the substrate which is inherent to microstrip antennas. Further details will be provided later.

To discretise integral eqn. 1 on an arbitrarily shaped patch, the vector-current basis functions, defined over triangular subdomains, are adopted. They were originally proposed in Reference 11 and developed further by Reference 12 for solving electromagnetic scattering problems. Each triangle is defined by an appropriate set of faces, edges, and vertices. Fig. 2 shows two triangles, T_n^+ and T_n^-, with the nth edge common between the two. The current to be determined is defined as flowing through the edge. Hence, a vector basis function associated with nth edge is

$$f_n(\boldsymbol{r}) = \begin{cases} \dfrac{l_n}{2A_n^+} \rho_n^+, & \boldsymbol{r} \text{ in } T_n^+ \\ \dfrac{l_n}{2A_n^-} \rho_n^-, & \boldsymbol{r} \text{ in } T_n^- \\ 0, & \text{otherwise} \end{cases} \tag{4}$$

and the current on the patch S may be approximated in terms of the f_n as

$$\boldsymbol{J} = \sum_{n=1}^{N} I_n f_n(\boldsymbol{r}) \tag{5}$$

where l_n is the length of the edge, $A_n^{\pm}$ is the area of triangle $T_n^{\pm}$ and N is the number of total unknown current coefficients.

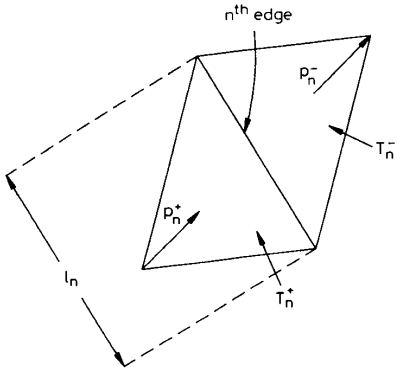

Fig. 2 *Local co-ordinates associated with an edge*

From the definition of the basis function one observes that at the boundary of the conjoined triangle pair T_n^+ and T_n^-, the current has no component normal to the boundary. This feature is ideally suited for applying boundary conditions to the current on a patch antenna. This follows because no component of the current is normal to the edge of either the patch antenna or its fedline. Furthermore, for a given triangular face, the three vector basis functions can form two independent vector basis functions. Finally a constant vector of arbitrary magnitude and direction within the triangle can be derived using a linear combination of the three vector basis functions.

The next step in the analysis is to reduce the operator type integral equation to its corresponding matrix form. The Galerkin procedure is used with the symmetric product defined by

$$\langle f, g \rangle = \iint_S f \cdot g\, dS \tag{6}$$

It follows that eqn. 1 may be converted to

$$\langle \boldsymbol{E}^s, f_m \rangle = j\omega \langle \boldsymbol{A}, f_m \rangle + \langle \nabla\Phi, f_m \rangle \tag{7}$$

Using a surface vector calculus identity, the last term in eqn. 7 can be rewritten as

$$\langle \nabla\Phi, f_m \rangle = -\iint_S \Phi \nabla_s f_m\, dS \tag{8}$$

where use has been made of the properties of f_m at the edges of S [12]. Eqn. 8 can now be approximated by

$$\langle \nabla\Phi, f_m \rangle = -l_m \left[\frac{1}{A_m^+} \iint_{T_m^+} \Phi \, dS - \frac{1}{A_m^-} \iint_{T_m^-} \Phi \, dS \right]$$
$$\approx -l_m [\Phi(r_m^{c+}) - \Phi(r_m^{c-})] \quad (9)$$

Similarly,

$$\left\langle \begin{Bmatrix} E^i \\ A \end{Bmatrix}, f_m \right\rangle = l_m \left[\frac{1}{2A_m^+} \iint_{T_m^+} \begin{Bmatrix} E^i \\ A \end{Bmatrix} \cdot \rho_m^+ \, dS + \frac{1}{2A_m^-} \iint_{T_m^-} \begin{Bmatrix} E^i \\ A \end{Bmatrix} \rho_m^- \, dS \right]$$
$$\approx \frac{l_m}{2} \left[\begin{Bmatrix} E^i(r_m^{c+}) \\ A(r_m^{c+}) \end{Bmatrix} \cdot \rho_m^{c+} + \begin{Bmatrix} E^i(r_m^{c-}) \\ A(r_m^{c-}) \end{Bmatrix} \cdot \rho_m^{c-} \right] \quad (10)$$

where the integrals are removed by approximating E^i and A by their values at the centroid of each triangle, which is shown in Fig. 3. With eqns. 9 and 10, eqn. 7

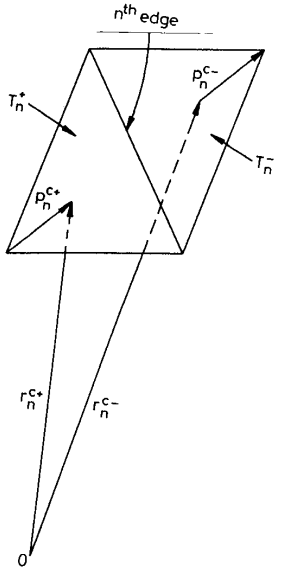

Fig. 3 *Geometry of the vectors to the centroids of the triangles that are associated with an edge*

becomes

$$j\omega l_m \left[A(r_m^{c+}) \cdot \frac{\rho_m^{c+}}{2} + A(r_m^{c-}) \cdot \frac{\rho_m^{c-}}{2} \right] + l_m [\Phi(r_m^{c-}) - \Phi(r_m^{c+})]$$
$$= l_m \left[E^i(r_m^{c+}) \cdot \frac{\rho_m^{c+}}{2} + E^i(r_m^{c-}) \cdot \frac{\rho_m^{c-}}{2} \right] \quad (11)$$

which is the equation associated with the edges of each triangle.

In this analysis the incident field is assumed to be generated by a delta-gap generator. This excitation model is fully discussed in Reference 8 and is based on the assumption that at a distance sufficiently far from both the generator and the radiating element the microstrip line supports only the quasi-TEM mode. Consequently, the right hand term of eqn. 10 may be written in a vector form $\{V\}$ with

$$v_i = \begin{cases} -E_0 & \text{at the position of the generator} \\ 0 & \text{otherwise} \end{cases}$$
$$i = 1, 2, \ldots, N \quad (12)$$

where E_0 is a constant related to the generator.

Substitution of the current expansion eqn. 5 into 11 yields an $N \times N$ matrix equation

$$[Z]\{I\} = \{V\} \quad (13)$$

where $\{I\}$ contains the unknown current coefficients I_n, which are defined by eqn. 5. The elements of column matrix $\{V\}$ are given by eqn. 12 and the elements of $[Z]$ are given by

$$Z_{mn} = l_m \left[j\omega \left(A_{mn}^+ \cdot \frac{\rho_m^{c+}}{2} + A_{mn}^- \cdot \frac{\rho_m^{c-}}{2} \right) + \Phi_{mn}^- - \Phi_{mn}^+ \right] \quad (14)$$

where

$$A_{mn}^{\pm} = \frac{\mu}{4\pi} \iint_s f_n(r') \cdot \overleftrightarrow{G}_A(r_m^{c\pm}, r') \, dS' \quad (15)$$

$$\Phi_{mn}^{\pm} = -\frac{1}{4\pi j\omega\varepsilon} \iint_s \nabla_s' \cdot f_n(r') G_q(r_m^{c\pm}, r') \, dS' \quad (16)$$

In fact, a t directed horizontal electric dipole embedded in a microstrip antenna generates a magnetic vector potential function with components only in the t and vertical directions. This is expressed by

$$\overleftrightarrow{G}_A = G_{At} tt + G_{Az} tz \quad (17)$$

As $\rho_m^{c\pm}$ is perpendicular to z, then eqn. 15 may be written simply as

$$A_{mn}^{\pm} = \frac{\mu}{4\pi} \iint_s f_n(r') \cdot G_{At}(r_m^{c\pm}, r') \, dS' \quad (18)$$

The current on the patch antenna and its feed line is obtained directly by multiplying both sides of eqn. 13 by Z^{-1}. The currents on the line sufficiently far from the perturbed zones form single-mode standing waves.

The single mode is the fundamental propagating mode; its characteristics are determined by the dimensions of the feed-line. Owing to an intrinsic property of vector basis functions, i.e. that only the current normal to the element edge is continuous, the current distribution on the feed line is not as smooth as it should be. However, transmission line theory still can be applied to compute the reflection coefficient at a given reference plane because all the necessary characteristics of the current distribution are represented correctly [13].

3 Potential Green's functions

As the spatial fields generated by electric dipoles are not uniform at the interfaces of microstrip substrates, nor at the air-substrate interface, matching of boundary conditions at these interfaces becomes difficult. To permit the field continuity conditions to be applied directly to these interfaces, the fields or the potentials must first be expanded into a continuous plane-wave spectrum (corresponding to a Fourier transform), or expanded into a continuous cylindrical-wave spectrum (corresponding to a Hankel transform). The Green's functions in eqns. 2 and 3 satisfy the microstrip boundary conditions; therefore they must incorporate an inverse transformation. In the present paper, Hankel transforms are used exclusively.

Next, we discuss the evaluation of the Green functions used in eqns. 16 and 18. In general, an arbitrarily shaped patch antenna is approximated by a number of triangular elements configured in some arbitrary arrangement.

Usually, no advantage can be derived from symmetry. For this reason, it is very important to calculate the potential Green's functions efficiently. The derivation of the Green's functions used in eqns. 16 and 18 have been extensively discussed in Reference 10. To extend the discrete image technique to electrically thin substrate, an infinite number of quasi image terms are extracted from the Green's function. These terms correspond to quasi-static field contributions and play an important role in the analysis of antennas with thin substrates. The potential Green's functions are then written as

$$G_{A_t}(r, r') = G_0 + k_0 \int_0^\infty T_1 \sum_{\exp} J_0(k_\rho \rho) \frac{k_\rho}{jk_{z1}} dk_\rho \tag{19}$$

$$G_q(r, r') = G_0 + G_{0n} + k_0 \int_0^\infty \left(T_1 + T_2 - K \sum_{n=1}^{\infty} (-K)^{n-1} \times e^{-j2(n-1)k_{z1}d} \right) \sum_{\exp} J_0(k_\rho \rho) \frac{k_\rho}{jk_{z1}} dk_\rho \tag{20}$$

where

$$G_0 = \frac{e^{-jk_1 r_0}}{r_0} - \frac{e^{-jk_1 r_0'}}{r_0'} \tag{21a}$$

$$r_0 = \sqrt{(\rho^2 + (z - z')^2)}$$

$$r_0' = \sqrt{(\rho^2 + (z + z')^2)}$$

$$\rho = \sqrt{((x - x')^2 + (y - y')^2)} \tag{21b}$$

$$G_{0n} = K \sum_{n=1}^{\infty} (-K)^{n-1} \left[\frac{e^{-jk_1 r_n'}}{r_n'} - \frac{e^{-jk_1 r_n''}}{r_n''} - \frac{e^{-jk_1 r_n'''}}{r_n'''} + \frac{e^{-jk_1 r_n''''}}{r_n''''} \right] \tag{21c}$$

with $K = (\varepsilon_r - 1)/(\varepsilon_r + 1)$.

The remaining quantities are defined as follows:

$$r_n' = \sqrt{(\rho^2 + (2nd + z + z')^2)}$$

$$r_n'' = \sqrt{(\rho^2 + (2nd + z - z')^2}$$

$$r_n''' = \sqrt{(\rho^2 + (2nd - z + z')^2)} \tag{21d}$$

$$r_n'''' = \sqrt{(\rho^2 + (2nd - z - z')^2)}$$

$$T_1 = \frac{R_{TE}}{1 + R_{TE} e^{-2jk_{z1}d}} \tag{21e}$$

$$T_2 = \frac{2(\varepsilon_r - 1)k_{z1}^2}{(k_{z0} + k_{z1})(\varepsilon_r k_{z0} + k_{z1}) \times (1 + R_{TE} e^{-j2k_{z1}d})(1 + R_{TM} e^{-j2k_{z1}d})} \tag{21f}$$

$$R_{TE} = \frac{k_{z1} - k_{z0}}{k_{z1} + k_{z0}} \quad R_{TM} = \frac{\varepsilon_r k_{z0} - k_{z1}}{\varepsilon_r k_{z0} + k_{z1}} \tag{21g}$$

$$\sum_{\exp} = e^{-jk_{z1}(2d + z + z')} - e^{-jk_{z1}(2d + z' - z')} - e^{-jk_{z1}(2d - z + z')} + e^{-jk_{z1}(2d - z - z')} \tag{21h}$$

where $k_{z0} = \sqrt{(k_0^2 - k_\rho^2)}$, $k_{z1} = \sqrt{(\varepsilon_r k_0^2 - k_\rho^2)}$. In the present paper, the Green's functions given by eqns. 19 and 20 are evaluated efficiently for different values of r and r', using the full-wave discrete image technique developed by Fang [10]. The advantage of this technique is that once the discrete images are found for a given substrate and frequency, the complex Sommerfeld-type integrals in eqns. 19 and 20 become a summation of a number of exponential functions (usually four or five is enough). This feature of the technique becomes important when the computational overhead for calculating the Green's functions is large. The underlying idea of this technique is the use of Prony's method to approximate the spectral domain Green's functions (the terms inside the brackets in eqns. 19 and 20) by a series of complex exponential functions. One starts the process by making an initial guess: this is then followed by a search for the optimal approximation using an optimisation procedure. The integration path used in the optimisation procedure, which is the same as that used in Prony's method, and time saving compared to other techniques, have been discussed in detail in Reference 10. Once the optimal approximations are determined, in terms of a series of complex exponential functions, the inverse transforms are easily carried out using the Sommerfeld identity.

It is worth mentioning that the term, G_{0n}, corresponds to the sum term inside the brackets of eqn. 20 and represents the quasistatic field contribution. For a substrate of ordinary thickness, only a few of the leading terms of the sum need to be retained. The accuracy that is achieved with the truncated series can easily be tested by comparing the results with those obtained using an exact integration. For the thin substrate, the quasistatic field is dominant; therefore, more quasi-static terms need to be retained so that an accurate result is realised.

4 Numerical remarks and numerical results

To demonstrate the above formulation and to validate the computer algorithms, numerical results are presented

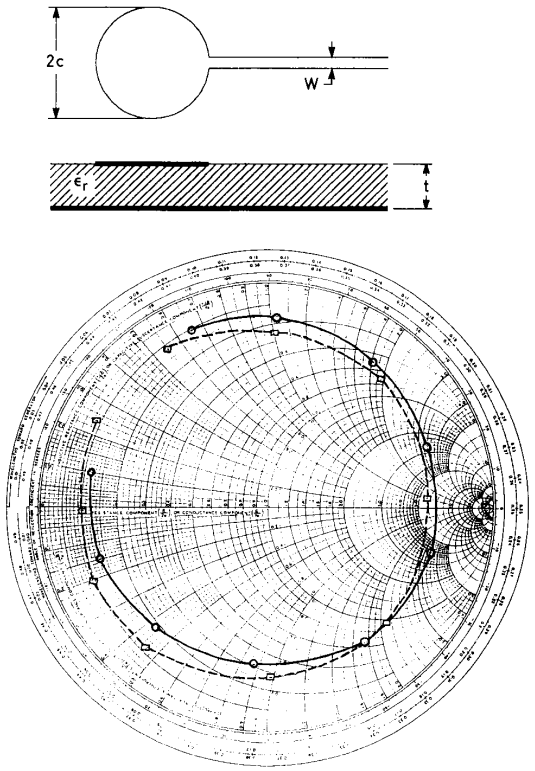

Fig. 4 *Computed and measured input impedance for an edge-fed circular patch antenna*

$c = 21.5$ mm $t = 1.59$ mm
$W/t = 2.86$ $\varepsilon_r = 2.2$
□- -□ computed 2.70–3.15 GHz clockwise
○—○ measured 0.05 GHz increment

for both microstrip line-fed circular patch antennas and triangular patch antennas. Fig. 4 shows a Smith chart plot of the calculated and the measured impedance loci for an edge-fed circular patch antenna. The measured data come from Reference 8, with the phase reference plane located at a distance of 96 ± 0.5 mm from the centre of the patch. The large uncertainties are due to the unavailability of accurate data for determining the characteristics of the coaxial to microstrip line connections*. The specified relative dielectric constant for the substrate material used for the measurement was 2.2. A value of 2.18, which is within the tolerance limits set by the manufacturer, was used for the calculations in order to achieve alignment between the frequencies of the computed data with those of the measured data.

As a second numerical example, proximity coupled patches are also analysed. Proximity coupled patch antennas have an advantage over end-coupled patches in that the overlap distance d may be used as an added variable for controlling the degree of coupling and matching. Also this type of feed provides a wider range of coupling coefficients with a reasonably large bandwidth. Also, proximity coupled patch antennas tend to have greater bandwidths than edge-fed ones, because of the increased substrate thickness between the radiator and the ground plane.

The surface of the circular patch and its feed-line is first modelled in terms of triangles with arbitrary edges and vertices arranged in such a manner as to replicate

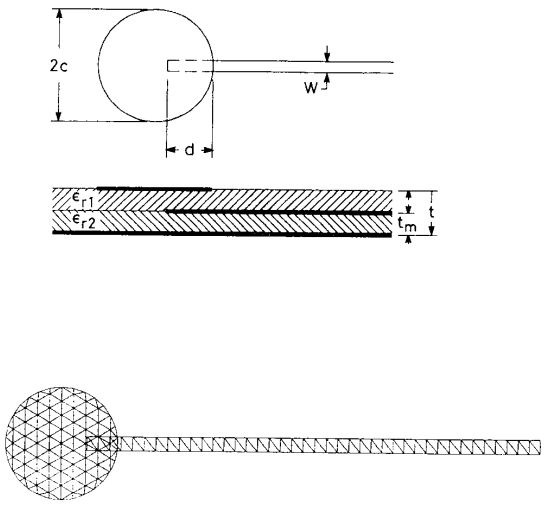

Fig. 5 *A proximity coupled circular patch antenna and the top view of the adopted pattern of triangles*
$c = 17.5$ mm $t = 3.18$ mm
$t_m = 1.59$ mm $W/t_m = 2.75$
$\epsilon_{r1}, \epsilon_{r2} = 2.62$

* DAVIDOVITZ, M.: Private communication, December 1989

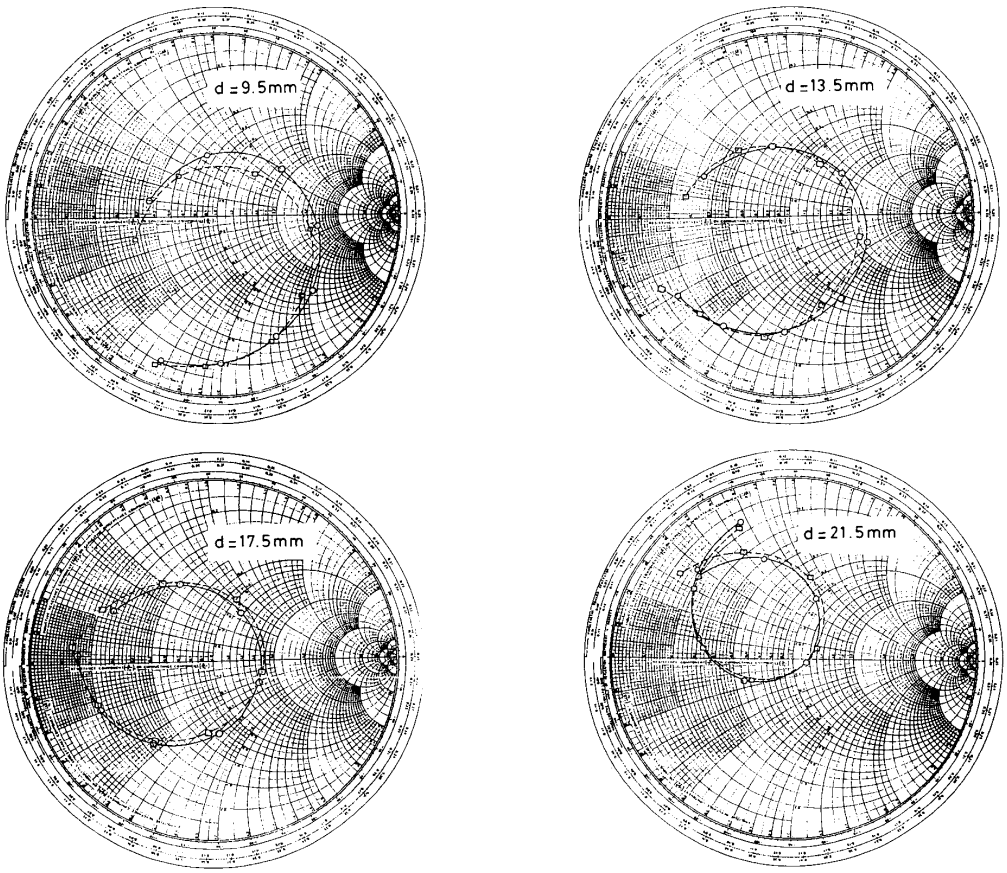

Fig. 6 *Computed and measured impedance for the proximity coupled circular patch*
□--□ computed 2.80–3.15 GHz clockwise
○—○ measured 0.05 GHz increment

the shape of the patch and line. Fig. 5 shows the top view of the adopted pattern of triangles. In this example there are a total of 218 triangular faces consisting of 271 edges. The unknown normal components of the electric currents are to be solved at the 271 edges. The input impedances that are derived using this technique are compared with measurements provided by Reference 8. Very good agreement is achieved for different overlap distances d, as can be seen in Fig. 6. We conclude that proximity coupled patch antennas can be accurately modelled by means of the proposed technique. It should be mentioned that the number of triangular elements is determined in such a way that a convergent result can be obtained.

The third example to be presented is a patch antenna with a thin substrate and a shape which corresponds to an equilateral triangle. Twenty quasistatic terms are extracted from the Green's function in order to obtain a discrete image approximation with sufficient accuracy. Convergent results are obtained using 258 triangular elements. These results involve 335 unknown currents. It can be seen in Fig. 7 that there is good agreement between the theoretical results obtained using our technique and experimental results obtained from Reference 14.

As an example of how one would use the full-wave numerical technique developed herein for designing a patch antenna, we investigate a proximity-coupled equilateral-triangle patch antenna. The choice of antenna is fairly arbitrary, but it will prove to be sufficient to the task of demonstrating the performance of the numerical technique for designing patch antennas with arbitrary shapes. Also, it will be seen that the technique takes into account the effects that any attending structures, such as feed lines, have on the performance of the antenna. The theoretical results will be compared with experimental measurements. It will be shown that the model predicts the performance of the antenna with a high degree of reliability.

In Fig. 8 a diagram of the antenna, as well as calculated and measured impedance loci is shown for two different values of d. From the Smith's charts in Fig. 8 it can be seen that by varying d one can improve the matching with little change in the resonant frequency. The reference point for the measurements was located 40 mm from the far end of feed line and lies beneath the patch antenna. The calibration for the measurements used the thru-reflect-line technique. Repeatable phase accuracy for the calibration standard was $\pm 2^\circ$ across the measured frequency range. For the data presented in Fig. 8, the repeatability of the measurements of $|S_{11}|$ averaged ± 0.05 dB with a repeatable phase of $\pm 4^\circ$. The quality of the calibration is discussed further in Reference 15.

The radiation pattern can be easily obtained by using the current distribution on the patch and the feed line and the results adopted from Reference 16. The calculated patterns include contributions from both the patch antenna and the feed line. The agreement between the measured and calculated E-plane patterns for the proximity coupled equilateral triangular patch antenna is fairly good, as shown in Fig. 9, where d is 5 mm and feed line length is about 64 mm. For purpose of comparisons, the calculated radiation pattern for a patch antenna without a feed line is also shown in Fig. 9. It is clear that the depression that occurs on broadside is caused by the feed line. The feed line perturbation varies with the length of feed line. This is especially true if the patch antennas are configured in the form of an array [17]. It should be noted that the cross-polarised component for the simu-

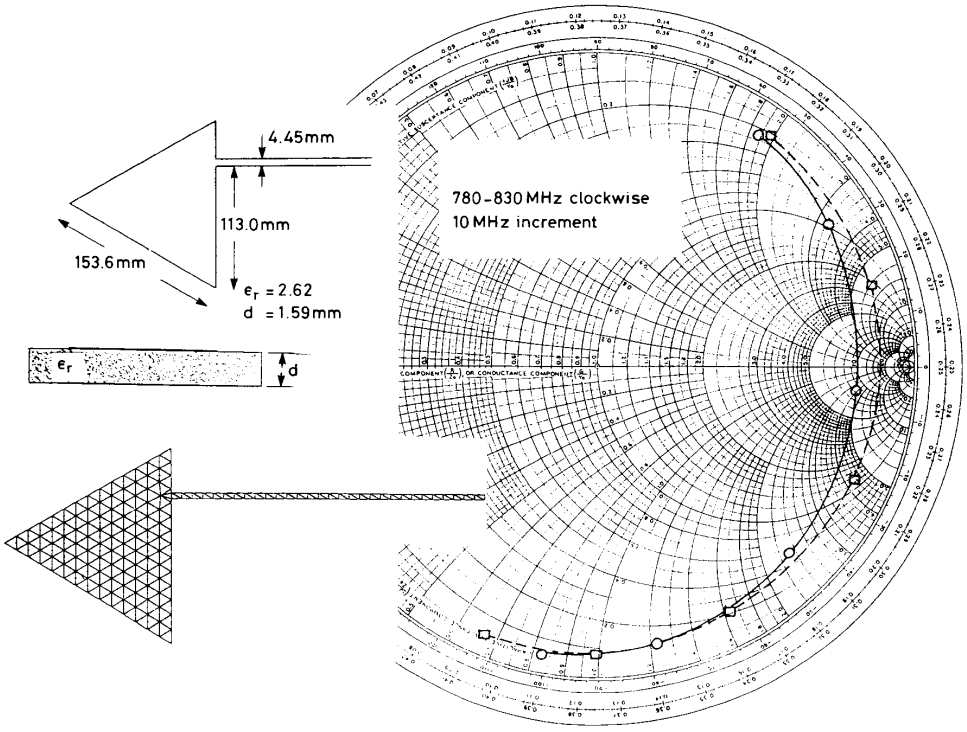

Fig. 7 *Computed and measured input impedance for an equilateral triangle line-fed patch with a top view of the triangle mesh*
□- -□ computed
○—○ measured

lated data is down by about 40 dB with respect to the copolarised component. The measured results show a value of about 35 dB for this quantity. The discrepancy between these two results is due to a limitation in the dynamic range of the anechoic chamber in which the data were recorded.

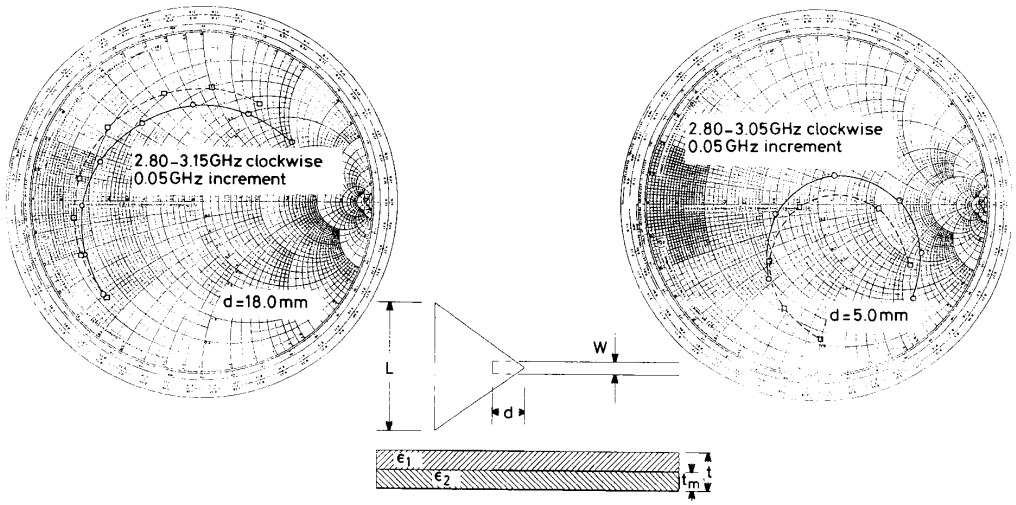

Fig. 8 *Computed and measured input impedance for a proximity coupled equilateral triangle patch* antenna
$L = 42.0$ mm $w = 4.55$ mm
$t = 3.18$ mm $\varepsilon_1 = \varepsilon_2 = 2.2$
$t_m = 1.59$ mm
□--□ computed
○—○ measured

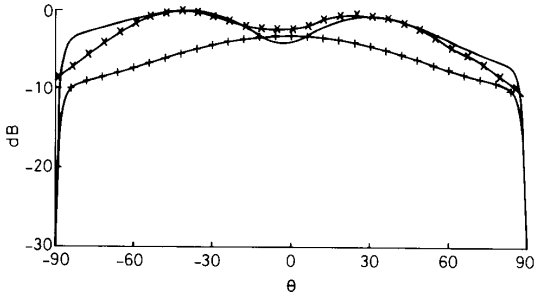

Fig. 9 *Radiation patterns of a proximity coupled equilateral triangle patch antenna with feed line length FL = 64 mm and FL = 0 mm*
——— FL = 64 mm
× × × FL = 64 mm (experiment)
+ + + FL = 0

5 Conclusions and discussions

A solution of the conventional electric field integral equation, whose formulation is based on a rigorous Green's function, was described. It was extended by incorporating the triangular finite element method so that this formulation can be used for carrying out numerical antenna design. It was shown that it is a flexible and accurate numerical tool which is able to handle arbitrarily shaped microstrip antennas with wide ranging frequency and substrate parameters.

The computer time required for generating the discrete images is negligible compared to the time required for filling the matrix. For a given substrate, only one set of images has to be found for each frequency, regardless of what antenna configuration needs to be analysed. Once the images are found, the original problem becomes a problem in free space.

It was noted that the elements of the matrix used in the solution can be easily generated by considering triangle element faces rather than edges. This reduces the computer time required for generating matrix elements by approximately a factor of nine. Although the Green's function presented here was derived for a substrate with a single layer, the extension to the multilayered problem is quite straightforward. The proposed technique provides a good quantitative description of the electric surface currents on the patch. This then allows related quantities such as, input impedance, the radiation pattern and polarisation purity to be accurately predicted. The work is being extended to other antenna problems, such as calculating the characteristics of arbitrarily shaped apertures or slots. In this case the magnetic current will be involved in unknown quantities.

6 Acknowledgments

The authors wish to thank Mr. Jian Wang for many helpful discussions. The authors also wish to thank Sharon R. Aspden of Rogers Corporation for providing the dielectric material used in this research under the auspices of their university program. Dr. M. Davidovitz is also acknowledged for providing some measurement details.

7 References

1 MOSIG, J.R., and GARDIOL, F.E.: 'General integral equation formulation for microstrip antennas and scatterers', *IEE Proc. H*, 1985, **132**, pp. 424–432
2 POZAR, D.M., and VODA, S.M.: 'A rigorous analysis of a microstrip fed patch antenna', *IEEE Trans.*, 1987, **AP-35**, pp. 1343–1349
3 CARVER, K.R., and COFFEY, E.L.: 'Theoretical investigation of the microstrip antenna'. Phys. Sci. Lab., New Mexico State Univ., PT-00929, Jan. 1979.

4 DERNERYD, A.G.: 'Analysis of the microstrip disk antenna element', *IEEE Trans.*, 1979, **AP-27,** pp. 660–664
5 SUZUKI, Y., and CHIBA, T.: 'Computer analysis method for arbitrarily shaped microstrip antenna with multiterminals', *IEEE Trans.*, 1984, **AP-32,** pp. 585–590
6 RICHARDS, W.F., LO, Y.T., and HARRISON, D.D.: 'An improved theory for microstrip antennas and applications', *IEEE Trans.*, 1981, **AP-29,** pp. 38–46
7 MARTINSON, T.M., and KUESTER, E.F.: 'Accurate analysis of arbitrarily shaped patch resonators on thin substrates', *IEEE Trans.*, 1988, **AP-36,** pp. 324–331
8 DAVIDOVITZ, M., and LO, Y.T.: 'Rigorous analysis of a circular patch antenna excited by a microstrip transmission line', *IEEE Trans.*, 1989, **AP-37,** pp. 949–958
9 DAMIANO, J.P., BENNEGUEOUCHE, J., and PAPIERNIK, A.: 'Study of multilayer microstrip antennas with radiating elements of various geometry', *IEE Proc. H*, 1990, **137,** pp. 163–170
10 FANG, D.G., YANG, J.J., and DELISLE, G.Y.: 'Discrete image theory for horizontal electric dipoles in a multilayered medium', *IEE Proc. H*, 1988, **135,** pp. 297–303
11 GLISSON, A.W.: 'On the development of numerical techniques for treating arbitrarily-shaped surfaces'. PhD dissertation, University of Mississippi, 1978
12 RAO, S.M.: 'Electromagnetic scattering and radiation of arbitrarily-shaped surfaces by triangular patch modelling'. PhD dissertation, Univ. of Mississippi, 1980
13 WU, K.L., and LITVA, J.: 'Full wave analysis of arbitrary shaped microstrip antennas by triangular finite element method'. IEEE AP-S Int. Symp. Digest, May 1990
14 LO, Y.T., SOLOMON, D., ORE, F.R., HARRISON, D.D., and DESCHAMPS, G.A.: 'Study of microstrip antennas, microstrip phased arrays, and microstrip feed networks'. Final Rep. RADC-TR-77-406, under contract AF19628-76-C-0140, Oct. 1977
15 FRALICH, R., WANG, J., and LITVA, J.: 'Enhanced precision microstrip antenna measurements with non-standard impedance lines at an arbitrary reference plane'. Technical report 228, Communication Research Laboratory, McMaster University, Ontario, Canada, 1991
16 YANG, H.Y., and ALEXOPOULOS, N.G.: 'Generation of nearly hemispherical and high gain azimuthally symmetric patterns with printed circuit antennas', *IEEE Trans.*, 1987, **AP-35,** pp. 972–977
17 WU, K.-L., SPENUK, M., LITVA, J., and FANG, D.-G.: 'Theoretical and experimental study of feed network effects on the radiation pattern of series-fed microstrip antenna arrays', *IEE Proc. H*, 1991, **138,** (3), pp. 238–242